

# Online Multi-Task Offloading for Semantic-Aware Edge Computing Systems

Xuyang Chen, *Student Member, IEEE*, Daquan Feng, *Member, IEEE*, Wei Jiang, *Associate Member, IEEE*, Qu Luo, *Member, IEEE*, Gaojie Chen, *Senior Member, IEEE*, and Yao Sun, *Senior Member, IEEE*

**Abstract**—Mobile edge computing (MEC) provides low-latency offloading solutions for computationally intensive tasks, effectively improving the computing efficiency and battery life of mobile devices. However, for data-intensive tasks or scenarios with limited uplink bandwidth, network congestion might occur due to massive simultaneous offloading nodes, increasing transmission latency, and affecting task performance. In this paper, we propose a semantic-aware multi-task offloading framework to address the challenges posed by limited uplink bandwidth. By introducing a semantic extraction factor, we balance the tradeoff among transmission latency, computation energy consumption, and task performance. To measure the offloading performance of different tasks, we design a unified and fair quality of experience (QoE) metric that includes execution latency, energy consumption, and task performance. We formulate the QoE optimization problem as a Markov decision process (MDP) and exploit the semantic-aware multi-agent proximal policy optimization (MAPPO) reinforcement learning algorithm to jointly optimize the semantic extraction factor and communication and computing resources allocation to maximize overall QoE. Experimental results show that the proposed method achieves a 12.68% improvement in user QoE compared with the semantic-unaware approach. Moreover, the proposed approach can be easily extended to models with different user preferences.

**Index Terms**—Mobile edge computing, resource allocation, task offloading, semantic-aware.

## I. INTRODUCTION

THE sixth generation (6G) of mobile communication is demonstrating its revolutionary potential, portending the arrival of an era of ultra-massive connectivity and the Internet of Things (IoT). The volume of data generated by a vast number of devices is experiencing an explosive surge. Various compute-intensive services, such as holographic communication, extended reality (XR), and autonomous driving continue to evolve, which increasingly burden user equipments (UEs) with heavy computational demands. However, the limited computational power and battery capacity of UEs make it challenging to support a multitude of computationally intensive

tasks. Cloud computing is considered capable of alleviating the computational pressure on UEs to some extent [1]. Offloading tasks to the cloud, which has abundant computing resources, significantly reduces local computational pressure. However, the high latency associated with cloud offloading is intolerable for latency-sensitive tasks. Furthermore, the centralized model of cloud computing poses data privacy and security issues. To address the aforementioned challenges, mobile edge computing (MEC) is considered an effective solution. Edge servers (ES) near the user can provide considerable computing and storage resources, which can be fully utilized by UEs distributed. Compared to cloud computing, MEC significantly reduces latency, while its distributed computing resources ensure user privacy and security.

Nevertheless, when tasks involve substantial data transfers, such as high-definition (HD) video processing [2], virtual reality (VR) applications [3], or real-time data analytics [4], the increased volume of data transmission imposes higher demands on channel quality to meet latency requirements. In such cases, semantic communication (SemCom) can provide an effective solution. SemCom, different from the traditional bit workflow based on Shannon's information theory [5], has demonstrated great potential for enhancing the efficiency and reliability of data transmission across various task scenarios, including text [6]–[8], image [9]–[11], video [12]–[14], XR [15]–[17], and multi-task [18]–[20]. By transmitting a compact semantic representation of task data, substantial bandwidth can be saved, ensuring high quality of service (QoS).

### A. Related Works

MEC technology has attracted widespread attention from academia and industry [21] due to its ability to enhance the computing capabilities of UEs and improve the quality of service (QoS). In [22], the authors optimized the allocation of communication, computation, and energy resources based on a perturbed Lyapunov algorithm, maximizing system throughput under the stability constraints of task and energy queues. A power minimization method with task buffer stability constraints was proposed in [23], where the Lyapunov optimization algorithm was used to solve computing offloading strategies. Liu et al. considered the requirements for ultra-reliable and ultra-low latency (URLLC) tasks [24], applying extreme value theory to minimize user power consumption while satisfying probabilistic queue length constraints.

However, the aforementioned model-based approaches are typically computationally intensive, further burdening user devices. Moreover, model-based methods often require multiple

Xuyang Chen is with the College of Electronics and Information Engineering, Shenzhen University, Shenzhen 518060, China, and also with the 5GIC & 6GIC, Institute for Communication Systems, University of Surrey, GU2 7XH Guildford, U.K. (email: chenxuyang2021@email.szu.edu.cn).

Daquan Feng is with the College of Electronics and Information Engineering, Shenzhen University, Shenzhen 518060, China (email: fdquan@szu.edu.cn).

Wei Jiang is with the Institute of Cyberspace Security, Zhejiang University of Technology, Hangzhou 310023, China (e-mail: weijiang@zjut.edu.cn).

Qu Luo and Gaojie Chen are with the 5GIC & 6GIC, Institute for Communication Systems, University of Surrey, GU2 7XH Guildford, U.K. (e-mail: : q.u.luo@surrey.ac.uk; gaojie.chen@surrey.ac.uk).

Yao Sun is with the James Watt School of Engineering, University of Glasgow, Glasgow, G12 8QQ, U.K. (email: Yao.Sun@glasgow.ac.uk).

iterations to find the optimal offloading strategy, which is intolerable for latency-sensitive tasks and impractical in rapidly changing wireless channel conditions. To address these issues, resource allocation and computation offloading methods based on Deep Reinforcement Learning (DRL) were proposed. The authors of [25] modeled the computation offloading as a multi-stage stochastic mixed-integer nonlinear programming (MINLP) problem and solved it using a combination of Lyapunov optimization and a DRL model, integrating the advantages of both model-based and DRL approaches. In [26], [27], the authors exclusively utilized DRL to solve for joint strategies of computation offloading and resource allocation, similarly achieving quite impressive results.

For services like holographic communication [28] and real-time video analysis [29], which are both latency-sensitive and compute-intensive, ensuring consistent QoS is challenging due to the need to transmit large amounts of data while combating wireless channel fading. Elaborate deep neural networks are often used for such sophisticated tasks, however, they also introduce significant computational and storage burdens on devices, necessitating the leverage of ES computing power through integration with MEC. Although offloading tasks to the ES can alleviate the computational burden on UEs and reduce execution latency, excessive data offloading or too many UEs offloading simultaneously can lead to network congestion, resulting in offloading failures.

Given these considerations, it is essential to design a semantic-aware MEC system by combining MEC with SemCom [30]. By performing semantic extraction on the data to be offloaded, UEs can filter out data irrelevant to the task, thereby reducing network traffic. In [31], the authors defined a semantic entropy to quantify the semantic information of different tasks. Deep Q-Network (DQN) and many-to-one matching algorithms are used to solve the joint optimization problem of semantic compression, channel allocation, and power distribution in multi-cell multi-task scenarios. A semantic-aware resource allocation method was proposed in [32], introducing a semantic-aware factor to characterize the relationship between semantic compression rate and computational overhead, aiming to balance the degree of semantic compression. The authors of [33] proposed a semantic-aware cloud-edge-end collaborative networking method to utilize distributed computing resources and also proposed a multi-task offloading system in [34], where a unified QoE metric was designed.

### B. Motivations and Contributions

In traditional MEC scenarios, computational and communication resources are often jointly optimized to minimize system energy consumption [35] or execution latency [36], or a combination of both [37]. However, these approaches lack consideration for task execution performance and comprehensive QoE. 6G strives to provide stable, reliable, and high-quality personalized services to each user [38]. Preferences often vary among different users and types of services. For instance, in MEC scenarios, users dealing with latency-sensitive tasks may prefer lower latency, those pursuing task performance may

favor better task execution accuracy, while users with limited battery power might opt for task offloading strategies that consume less power. Therefore, a good QoE metric should encompass the preferences of different users. Additionally, since each user may need to handle different tasks, the complexity and evaluation metrics of different tasks vary. For example, bimodal tasks like visual question answering (VQA) typically require more processing time and computational resources compared to text translation, and their evaluation metrics are entirely different.

Semantic-aware MEC systems have been studied in [31]–[34]. Nonetheless, in [31]–[33], the authors did not consider multi-tasks, limiting their ability to compare users engaged in different types of tasks. The authors of [34] did not consider the impact of semantic extraction on task execution latency and performance. To address the aforementioned challenges, we investigate resource allocation schemes in multi-task offloading that coordinate computational and communication resources through semantic compression-aware methods. To fairly compare the offloading performance of different task types, a unified QoE metric is proposed. Computational and communication resources are jointly optimized to maximize the overall QoE for UEs. The main contributions of this paper are summarized as follows:

- We propose a novel semantic-aware task offloading system for multi-tasks. The SemCom systems for image classification, text classification, and VQA are first constructed to compress source data into compact semantic representations. The semantic extraction factor is used to characterize the degree of data compression, which affects the task's execution latency, energy consumption, and performance.
- We design a unified and fair QoE evaluation metric that addresses the challenges posed by the diverse distribution of user task types and the lack of uniform task evaluation criteria. Specifically, the QoE metric comprises three components: task execution latency, task execution energy consumption, and task execution performance. We employ a unified logistic function to normalize these three components, thereby obtaining a unified and comparable QoE.
- The joint optimization for semantic extraction factor, computational resources, and communication resources is performed using the semantic-aware MAPPO algorithm, maximizing the overall QoE. Users solve for the optimal channel allocation, power allocation, semantic extraction level, and computation offloading scheme according to their observed task sizes and channel conditions.
- Comprehensive experiments demonstrate the effectiveness of the proposed approach. Compared to the semantic-unaware method, the proposed algorithm demonstrates a 12.68% improvement in user QoE. Additionally, the proposed approach can meet user preferences for various metrics such as execution latency, energy consumption, and execution performance.

The remainder of this paper is organized as follows. Section II describes the semantic-aware transmission and computation

model, defines the unified QoE metric, and formulates the problem as maximizing overall QoE. Section III introduces solving the QoE maximization problem using the MAPPO algorithm, providing training details. Section IV presents relevant experimental details and simulation results. Finally, Section V outlines our conclusions.

## II. SYSTEM MODEL AND PROBLEM FORMULATION

We propose a novel semantic-aware multi-task offloading system, as shown in Fig. 1, where UEs employ an orthogonal frequency-division multiple access (OFDMA) scheme. At the access point (AP),  $K$  resource blocks are allocated to serve  $N$  users at different sub-channels. The set of UEs and sub-channels are defined as  $\mathcal{N} = \{1, 2, \dots, N\}$  and  $\mathcal{K} = \{1, 2, \dots, K\}$ . The length of the  $UE_n$ 's task queue is denoted as  $Q_n$ . The task currently being executed by the  $UE_n$  is represented by  $q_n^{\mathcal{M}}$ , where  $\mathcal{M} \in \{task_1, task_2, \dots, task_m\}$ . Hence, each UE may contain up to  $m$  different types of tasks. We assume that tasks are atomic [34], i.e., all tasks are either executed locally or offloaded to the ES. The illustrations of the main notations are summarized in Table I.

### A. Semantic-Aware Model

Traditional MEC offloading methods usually require transmitting all data to the ES. SemCom enables the extraction of task-relevant semantic information, reducing bandwidth consumption while enhancing robustness to channel variations. Based on this, we propose a semantic-aware multi-task offloading framework. Fig. 2 illustrates the process of semantic-aware offloading. While semantic extraction indeed reduces the volume of data transmitted, the associated increase in semantic extraction latency and computational burden must also be comprehensively considered. Hence, we define a semantic extraction factor  $\mu_n \in [\mu_n^{min}, 1]$ . The semantic extraction module determines the level of data compression. When  $\mu_n = 1$ , the UE transmits all data instead of semantic information. Transmitting all data can achieve better task performance, but it imposes a heavy transmission burden. The smaller the  $\mu_n$ , the greater the level of semantic compression, which significantly reduces the transmission load. However, semantic extraction introduces additional computational overhead and may decrease task performance on the ES. The minimum value  $\mu_n^{min}$  is typically determined by task accuracy requirements and user battery capacity. Therefore, selecting  $\mu_n$  requires a comprehensive evaluation of the current task computational load, channel environment, user battery capacity, and other relevant information.

### B. Transmission Model

The channel gain from  $UE_n$  to ES via sub-channel  $k$  is denoted by  $|g_{k,n}|^2 = |h_{k,n}|^2/d_n^{-\alpha}$ , where  $h_n \sim \mathcal{CN}(0, 1)$  is Rayleigh fading coefficient, and  $d_n$  is the distance from  $UE_n$  to ES, and  $\alpha$  is the path loss exponent, and  $\mathcal{CN}(0, 1)$  is the complexed Gaussian distribution with zero mean and variance

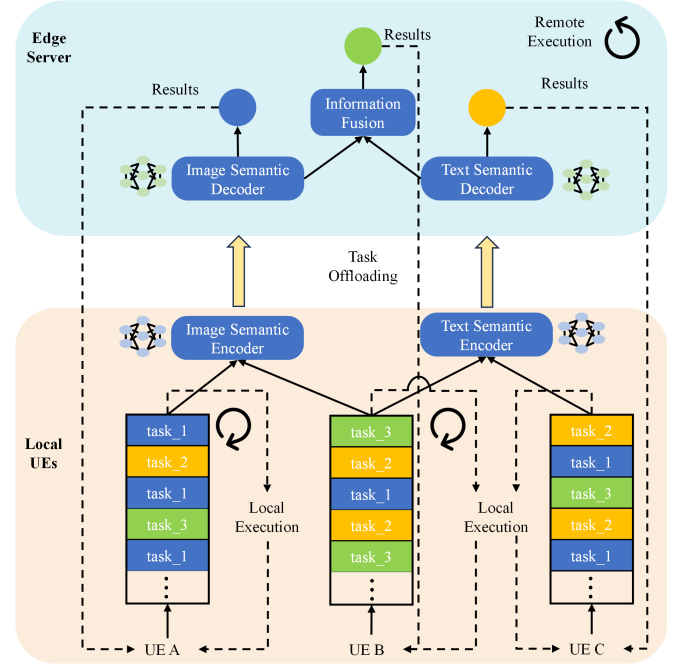


Fig. 1. Semantic-aware multi-task offloading system model. Each task is fed into a semantic codec specifically designed for its type.

one. The maximum achievable offloading data rate from  $UE_n$  to ES can be represented as

$$R_n = \sum_{k=1}^K B \log_2 \left( 1 + \frac{x_{k,n} |g_{k,n}|^2 p_n}{\sigma_z^2} \right), \quad (1)$$

where  $B$  is the sub-channel bandwidth, and  $p_n$  denotes the transmit power from  $UE_n$  to ES, and  $\sigma_z^2$  is the additive white Gaussian noise (AWGN) noise power.  $x_{k,n}$  denotes the sub-channel allocation indicators.  $x_{k,n} = 1$  indicates  $UE_n$  is assigned to sub-channel  $k$ ,  $x_{k,n} = 0$  otherwise. Therefore, the transmission latency can be expressed as

$$t_n = \frac{\rho_n s_n \mu_n^p}{R_n}, \quad (2)$$

where  $s_n$  is the normalized transmission data from  $UE_n$  to ES, and  $p > 0$  is a constant parameter.  $\rho_n$  is an offload indicator, where  $\rho_n = 1$  represents offloading tasks to ES, and  $\rho_n = 0$  denotes local computation. Compared to the amount of data required for task offloading, the computation results typically involve a much smaller data size [39], [40], therefore, we only consider the upload rate and latency.

### C. Computation Model

Each task can be executed in one of three modes: locally on the device, directly offloaded to the ES ( $\mu_n = 1$ ), or semantically pre-processed locally and then offloaded ( $\mu_n^{min} \leq \mu_n < 1$ ). The latency incurred by semantic extraction at the user should be considered in the overall task execution time. Therefore, the computation latency of  $UE_n$  can be denoted as

$$t_n^U = \begin{cases} \frac{(1-\rho_n)t_n^U}{c_n}, & \text{if } \mu_n = 1, \\ \frac{(1-\rho_n)t_n^U}{c_n} + \frac{\rho_n t_n^{SE}}{\mu_n^q c_n}, & \mu_n^{min} \leq \mu_n < 1, \end{cases} \quad (3)$$

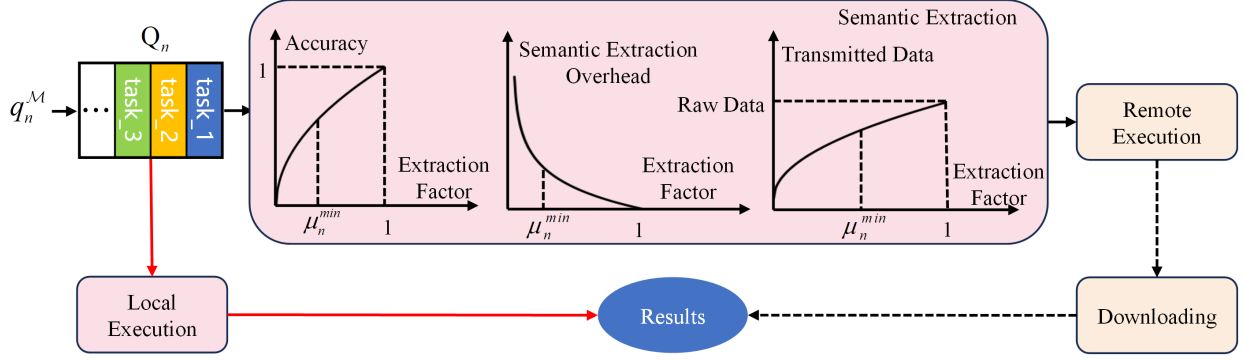


Fig. 2. Semantic extraction workflow. The semantic extraction factor alters the degree of semantic compression, affecting the computational burden of semantic extraction, the volume of data transmission, and the accuracy of task execution.

TABLE I  
NOTATIONS AND SYMBOLS

Notation	Explanation
$\mathcal{N}$	The set of all UEs
$\mathcal{K}$	The set of all sub-channels
$\mathcal{M}$	The set of task types
$\mu_n$	The semantic extraction factor
$Q_n$	The task length of UE <sub>n</sub>
$q_n^M$	The task currently being executed
$g_{k,n}$	The channel gain from UE <sub>n</sub> to ES via sub-channel $k$
$R_{k,n}$	The maximum offloading rate from UE <sub>n</sub> to ES via sub-channel $k$
$B$	The channel bandwidth
$\rho_n$	The offloading decision
$s_n$	The transmitted message
$t_n$	The transmission latency
$t_n^U$	The computation time of UE <sub>n</sub>
$l_n^U$	The GPU consumption executed by UE <sub>n</sub>
$l_n^{SE}$	The basic GPU consumption of semantic extraction
$c_n$	The GPU computation capability of UE <sub>n</sub>
$t^S$	The computation time of ES
$l_n^S$	The GPU consumption executed by ES
$c_s$	The GPU computation capability of ES
$t_n^M$	The execution time of task $q_n^M$
$E_n^U$	The energy consumption of UE <sub>n</sub>
$\kappa^U$	The energy coefficient of UE <sub>n</sub>
$f_n$	The GPU clock frequency of UE <sub>n</sub>
$E^S$	The energy consumption of ES
$\kappa^S$	The energy coefficient of ES
$f_s$	The GPU clock frequency of ES
$\varepsilon_n^M$	The accuracy of task $\mathcal{M}$
$QoE_n$	The QoE of UE <sub>n</sub>
$G_{\mathcal{M}}^t, G_{\mathcal{M}}^e, G_{\mathcal{M}}^a$	The functions of execution time, energy consumption, and task accuracy score, respectively
$\omega_t, \omega_e, \omega_a$	The weights of execution time, energy consumption, and task accuracy, respectively

where  $q > 0$  is a constant parameter,  $l_n^U$  is the Graphic Processing Unit (GPU) consumption of the current task computed by UE<sub>n</sub>, and  $l_n^{SE}$  is the basic GPU consumption of semantic extraction.  $l_n^U$  and  $l_n^{SE}$  are related to the corresponding task  $\mathcal{M}$ .  $k > 0$  is a constant parameter.  $c_n = \alpha_{ma} N_U f_n$  is the GPU computation capability of UE<sub>n</sub>.  $\alpha_{ma} = 2$  corresponds to the floating-point operations (FLOPs) per cycle per core (FLOPs/cycle/core), where each instruction executes a fused multiply-add (FMA) operation.  $N_u$  represents the number of

CUDA cores available on UE<sub>n</sub>.  $f_n$  denotes the GPU clock frequency of UE<sub>n</sub>. When tasks are offloaded to ES, the computation time of tasks on the ES can be expressed as

$$t^S = \sum_{n=1}^N \frac{l_n^S}{c_s}, \quad (4)$$

where  $c_s = N_S f_s \alpha_{ma}$  is the GPU computation capability of ES.  $l_n^S$  is the GPU consumption of the task offloaded by the UE<sub>n</sub> to the ES.  $N_s$  denotes the number of CUDA cores available on ES.  $f_s$  denotes the GPU clock frequency of ES. ES allocates its computational resources among users fairly, proportional to the amount of computation offloaded by each user. Combining the aforementioned factors, the processing latency of UE<sub>n</sub>'s current task  $q_n^M$  can be expressed as

$$\begin{aligned} t_n^M &= \rho_n(t_n + t_n^U + t^S) + (1 - \rho_n)t_n^U \\ &= \rho_n(t_n + t^S) + t_n^U. \end{aligned} \quad (5)$$

#### D. Energy Consumption Model

The energy consumption of UE<sub>n</sub> can be written as

$$E_n^U = \kappa^U t_n^U f_n^3 + p_n t_n, \quad (6)$$

where  $\kappa^U$  is the energy coefficient of UE<sub>n</sub>. The energy consumption of ES can be described as [34]

$$E^S = \kappa^S t^S f_s^3, \quad (7)$$

where  $\kappa^S$  is the energy coefficient of ES. Therefore, the energy consumption of UE<sub>n</sub>'s current task  $q_n^M$  can be expressed as

$$E_n^M = E_n^U + E^S. \quad (8)$$

#### E. Multi-Task Offloading Design and Problem Formulation

The execution performance of all tasks in the task queue is represented as

$$\varepsilon_n^M = f^M(s_n, \nu_n), \quad (9)$$

where  $\varepsilon_n^M$  is the accuracy of task  $\mathcal{M}$ , and  $f^M(\cdot)$  is the pretrained semantic transmission model for task  $\mathcal{M}$ , and  $\nu_n$  is SNR. Once the model training is completed, we can directly calculate the number of FLOPs required by the UE's semantic encoder to determine the basic GPU consumption  $l_n^{SE}$  for semantic extraction. Similarly, we compute the number of

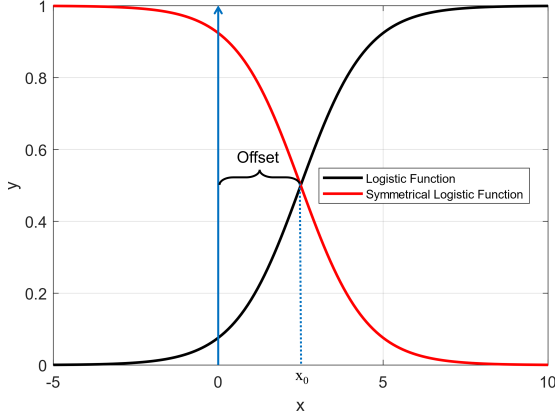


Fig. 3. QoE function. The logistic function serves as the scoring function for task accuracy, with its symmetric function scoring execution latency and energy consumption. The offset  $x_0$  represents the latency, energy consumption, or task accuracy of local execution.

FLOPs required by the ES's semantic decoder to determine the GPU consumption  $l_n^S$  for the ES. To evaluate the performance of offloading tasks for different UEs, it is essential to define a unified QoE standard.

The performance of task execution is associated with computation time, energy consumption, and task accuracy. However, defining a fair and reasonable QoE is challenging. When tasks of different types are unevenly distributed among different UEs, directly calculating the weighted sum of energy consumption, computation time, and task accuracy is unfair. Typically, text tasks have lower computation time and energy consumption than image tasks, while image tasks have lower computation time and energy consumption than VQA tasks. Additionally, the accuracies of different tasks are usually incomparable. Inspired by [41]–[43], we propose a QoE calculation method that can fairly compare task execution performance across different UEs:

$$\begin{aligned} \text{QoE}_n &= \frac{1}{Q_n} \sum_{q_n^{\mathcal{M}}=1}^{Q_n} (\omega_t G_{\mathcal{M}}^t + \omega_e G_{\mathcal{M}}^e + \omega_a G_{\mathcal{M}}^a) \\ &= \sum_{q_n^{\mathcal{M}}=1}^{Q_n} \left( \frac{\omega_t}{1 + e^{-\lambda(t_n^l - t_n^{\mathcal{M}})}} + \frac{\omega_e}{1 + e^{-\beta(E_n^l - E_n^{\mathcal{M}})}} \right. \\ &\quad \left. + \frac{\omega_a}{1 + e^{-\eta(\varepsilon_n^{\mathcal{M}} - \varepsilon_n^l)}} \right), \end{aligned} \quad (10)$$

where  $\omega_t$ ,  $\omega_e$ , and  $\omega_a$  are the weights of computation time, energy consumption, and task accuracy, respectively. The sum of  $\omega_t$ ,  $\omega_e$  and  $\omega_a$  are equal to 1.  $Q_n$  is the task length of  $\text{UE}_n$ .  $t_n^l = l_n^U / c_n$  denotes the task execution delay by  $\text{UE}_n$ . As shown in Fig. 3, we use the logistic/sigmoid function and its symmetrical counterpart for QoE calculations. Corresponding latency score  $G_{\mathcal{M}}^t$  and energy consumption score  $G_{\mathcal{M}}^e$  are calculated using the symmetric logistic function, while accuracy score  $G_{\mathcal{M}}^a$  is measured with the logistic function. The offset  $x_0$  represents local execution latency, energy consumption, or accuracy. Specifically,  $E_n^l = \kappa^U t_n^l (f_n)^3$  denotes the task execution energy consumption by  $\text{UE}_n$ .  $\varepsilon_n^l$  denotes the task execution accuracy by  $\text{UE}_n$ . That is, we normalize the QoE

using the latency, energy consumption, and accuracy of tasks executed locally by the UE.

Mathematically, the optimization problem can be formulated as

$$(\mathbf{P0}) \quad \underset{\{\rho, \mathbf{p}, \mathbf{f}, \mathbf{x}, \boldsymbol{\mu}\}}{\text{maximize}} \quad \sum_{n=1}^N \text{QoE}_n \quad (11a)$$

$$\text{s.t.} \quad \rho_n \in \{0, 1\}, \quad \forall n \in \mathcal{N}, \quad (11b)$$

$$x_{k,n} \in \{0, 1\}, \quad \forall n \in \mathcal{N}, \forall k \in \mathcal{K}, \quad (11c)$$

$$\sum_{k=1}^{\mathcal{K}} x_{k,n} = 1, \quad \forall n \in \mathcal{N}, \quad (11d)$$

$$\sum_{n=1}^{\mathcal{N}} x_{k,n} = 1, \quad \forall k \in \mathcal{K}, \quad (11e)$$

$$\mu_n^{\min} \leq \mu_n \leq 1, \quad \forall n \in \mathcal{N}, \quad (11f)$$

$$p_n \leq p_{\max}, \quad \forall n \in \mathcal{N}, \quad (11g)$$

$$f_n \leq f_{\max}, \quad \forall n \in \mathcal{N}, \quad (11h)$$

$$t_n^{\mathcal{M}} \leq t_{\max}, \quad \forall n \in \mathcal{N}, \quad (11i)$$

$$E_n^{\mathcal{M}} \leq E_n^{\max}, \quad \forall n \in \mathcal{N}, \quad (11j)$$

$$\varepsilon_n^{\mathcal{M}} \geq \varepsilon_{\min}, \quad \forall n \in \mathcal{N}, \quad (11k)$$

where  $\{\rho, \mathbf{p}, \mathbf{f}, \mathbf{x}, \boldsymbol{\mu}\} = \{\rho_n, p_n, f_n, x_{k,n}, \mu_n\}, \forall n \in \mathcal{N}, \forall k \in \mathcal{K}$ .  $\mathbf{x} \in \mathbb{R}^{K \times N}$  denote the collection of all sub-channel allocation indicators  $x_{k,n}$ .  $x_{k,n} = 1$  indicates  $\text{UE}_n$  is assigned to sub-channel  $k$ ,  $x_{k,n} = 0$  otherwise. In  $(\mathbf{P0})$ , (11b) and (11c) represent the offloading choice and channel selection constraints, respectively. Constraints (11d) and (11e) indicate that each UE is assigned to one sub-channel and each sub-channel is occupied by one UE.  $p_{\max}$  in (11g) is the maximum transmit power constraint,  $f_{\max}$  in (11h) is the maximum GPU frequency of  $\text{UE}_n$ ,  $t_{\max}$  in (11i) is the maximum execute latency constraint,  $E_n^{\max}$  in (11j) is the battery capacity of  $\text{UE}_n$ , and  $\varepsilon_{\min}$  in (11k) is the minimum task accuracy requirement, which is dependent on the task type  $\mathcal{M}$  of the current task.

### III. MULTI-AGENT PROXIMAL POLICY OPTIMIZATION FOR RESOURCE ALLOCATION

The binary offloading variable in Constraint (11b) introduces non-convexity, and the QoE is characterized by a non-convex logistic function, rendering the problem  $\mathbf{P0}$  a non-convex MINLP problem. To solve the non-convex MINLP problem  $\mathbf{P0}$ , we propose an advanced semantic-aware MAPPO algorithm, i.e., an actor-critic-based reinforcement learning algorithm, which is suitable for both discrete and continuous action spaces. To utilize the semantic-aware MAPPO algorithm, we reformulate problem  $\mathbf{P0}$  as an MDP and detail the training process of the MAPPO.

#### A. Problem Reformulation Based on MDP

A 4-tuple MDP  $\langle \mathcal{S}, \mathcal{A}, \mathcal{R}, \gamma \rangle$  is used to describe the interaction between the ES and the wireless network, where  $\mathcal{S}$ ,  $\mathcal{A}$ ,  $\mathcal{R}$  and  $\gamma \in [0, 1)$  denote the state space, action space, reward function, and the discount factor, respectively. As agents, UEs

need to collect observable states to input into the policy network and obtain their actions. After executing actions, UEs update their observable states and the policy network based on corresponding rewards to improve the output of actions. Specifically, the observable state of UE<sub>n</sub> can be represented as  $o_n = \{g_{k,n}, l_n^U, l_n^S\} \in \mathcal{S}$ . The action space of UE<sub>n</sub> refers to the variables that need to be optimized, which can be expressed as  $a_n = \{\rho_n, p_n, f_n, \mu_n, x_{k,n}\} \in \mathcal{A}$ . UEs need to continuously optimize offloading strategies, transmit power, local computation frequency, semantic compression ratio, and channel assignment to purchase better QoE. Drawing from the optimization problem **P0**, it is evident that the reward function needs to focus on the summation QoE of all UEs. In addition to QoE, the reward function includes penalty terms for latency and task accuracy, expressed as

$$r_n = \begin{cases} QoE_n & \text{successful task execution,} \\ t_{max} - t_n & \text{if (11i) not satisfied,} \\ E_n^{max} - E_n^{\mathcal{M}} & \text{if (11j) not satisfied,} \\ \varepsilon_n^{\mathcal{M}} - \varepsilon_{min} & \text{if (11k) not satisfied.} \end{cases} \quad (12)$$

Therefore, the total reward at the  $t$ th training timestep is defined as  $r_t = \sum_{n=1}^N r_n$ . The cumulative long-term reward accounts for the impact of the current state and action on the expected future rewards:

$$R_t(\tau) = \sum_{t'=t}^T \gamma^{t'-t} r_{t'}, \quad (13)$$

where  $\tau$  is a completed trajectory. Let  $\pi_{\theta}$  represents a policy parameterized by  $\theta$ , where  $\mathbf{a}_t$  is the collection of  $a_n$  at time  $t$ , and  $\mathbf{s}_t$  is the collection of  $o_n$  at time  $t$ . Given the state  $\mathbf{s}_t$ , the probability of taking action  $\mathbf{a}_t$  under policy  $\pi_{\theta}$  is denoted as  $\Pr(\mathbf{a}_t | \mathbf{s}_t, \pi_{\theta})$ . Consequently, the expected discounted rewards under policy  $\pi_{\theta}$ , denoted as  $J(\pi_{\theta})$ , can be expressed as

$$J(\pi_{\theta}) = \mathbb{E}_{\mathbf{a}_t \sim \pi_{\theta}, \mathbf{s}_t \sim \mathcal{P}} \left[ \sum_{t=1}^T \gamma^{t-1} r_t(\mathbf{s}_t, \mathbf{a}_t) \right]. \quad (14)$$

UEs seek to find the optimal policy  $\pi_{\theta}$  to maximize the expected cumulative reward  $J(\pi_{\theta})$ . Therefore, the optimization problem **P0** is reformulated as an MDP problem:

$$\begin{aligned} \max_{\pi_{\theta}} & J(\pi_{\theta}) \\ \text{s.t.} & \mathbf{a}_t \sim \pi_{\theta}(\mathbf{a}_t | \mathbf{s}_t), \mathbf{s}_{t+1} \sim \Pr(\mathbf{s}_{t+1} | \mathbf{s}_t, \mathbf{a}_t). \end{aligned} \quad (15)$$

### B. Semantic-aware MAPPO Algorithm

Fig. 4 illustrates our proposed MAPPO algorithm. PPO is an on-policy algorithm whose trajectories are typically sampled using a fixed policy  $\pi_{\theta}$ , and policy updates are made using only those trajectories sampled by  $\pi_{\theta}$ . It utilizes an experience replay buffer, which stores trajectories from past time steps. To enhance environmental exploration efficiency, the MAPPO algorithm employs a parallelized architecture with multiple threads that simultaneously collect environment interaction data and synchronize it during updates. To enhance data efficiency, the MAPPO algorithm typically uses small batches of data for multi-step updates. This leads to a slight discrepancy between the current policy and the policy used

during data generation during the update process. The use of importance sampling techniques allows for the assessment of this policy deviation and adjusts the gradient updates, thus stabilizing the learning process. The importance sampling is outlined in *Lemma 1*.

*Lemma 1.* Given distributions  $x \sim p(x)$  and  $x \sim q(x)$ , the  $\mathbb{E}_{x \sim p} f(x) = \mathbb{E}_{x \sim q} \frac{p(x)}{q(x)} f(x)$ .

*Proof.* Given  $x \sim p(x)$ , the expectation of  $f(x)$  can be expressed as

$$\begin{aligned} \mathbb{E}_{x \sim p} f(x) &= \int_x p(x) f(x) dx \\ &= \int_x \frac{p(x)}{q(x)} q(x) f(x) dx = \mathbb{E}_{x \sim q} \frac{p(x)}{q(x)} f(x). \end{aligned} \quad (16)$$

Using importance sampling, the optimization function for PPO can be reformulated as

$$J^{\theta'}(\theta) = \mathbb{E}_{(\mathbf{s}_t, \mathbf{a}_t) \sim \pi_{\theta'}} \left[ \frac{p_{\theta}(\mathbf{a}_t | \mathbf{s}_t)}{p_{\theta'}(\mathbf{a}_t | \mathbf{s}_t)} A_t^{\theta'}(\mathbf{s}_t, \mathbf{a}_t) \right], \quad (17)$$

where  $\theta$  is the parameter that needs to be optimized while  $\theta'$  is the parameter used for sampling.  $p_{\theta}(\mathbf{a}_t | \mathbf{s}_t)$  and  $p_{\theta'}(\mathbf{a}_t | \mathbf{s}_t)$  represent taking action  $\mathbf{a}_t$  given state  $\mathbf{s}_t$  with  $\theta$  and  $\theta'$ , respectively.  $\theta'$  interacts with the environment to generate trajectories while  $\theta$  does not interact with the environment directly but learns from the trajectories sampled by  $\theta'$ . The advantage function  $A^{\theta'}(\mathbf{s}_t, \mathbf{a}_t)$  represents the advantage of state-action pairs  $(\mathbf{s}_t, \mathbf{a}_t)$  obtained through the interaction of  $\theta'$  with the environment, which is defined as

$$A_t^{\theta'}(\mathbf{s}_t, \mathbf{a}_t) = Q_t^{\theta'}(\mathbf{s}_t, \mathbf{a}_t) - V_t^{\theta'}(\mathbf{s}_t). \quad (18)$$

The state-action value function  $Q_t^{\theta'}(\mathbf{s}_t, \mathbf{a}_t)$  is represented as

$$Q_t^{\theta'}(\mathbf{s}_t, \mathbf{a}_t) = \mathbb{E}_{\mathbf{a}_t \sim \pi_{\theta'}, \mathbf{s}_t \sim \mathcal{P}} \left[ \sum_{t'=t}^T \gamma^{t'-t} r_{t'} \right], \quad (19)$$

and the state-value function is defined as

$$V_t^{\theta'}(\mathbf{s}_t) = \mathbb{E}_{\mathbf{s}_t \sim \mathcal{P}} \left[ \sum_{t'=t}^T \gamma^{t'-t} r_{t'} \right]. \quad (20)$$

It is noted that  $Q_t^{\theta'}(\mathbf{s}_t, \mathbf{a}_t)$  can also be expressed by temporal difference (TD) form as  $Q_t^{\theta'}(\mathbf{s}_t, \mathbf{a}_t) = r_t + \gamma V_t^{\theta'}(\mathbf{s}_{t+1})$ . Therefore, (18) can be reformulated as

$$A_t^{\theta'}(\mathbf{s}_t, \mathbf{a}_t) = r_t + \gamma V_t^{\theta'}(\mathbf{s}_{t+1}) - V_t^{\theta'}(\mathbf{s}_t). \quad (21)$$

However, estimating based on TD often carries a higher bias. Thus, we employ Generalized Advantage Estimation (GAE) [44] to evaluate the current state-action value function. The GAE advantage function can be expressed as

$$A^{GAE}(\mathbf{s}_t, \mathbf{a}_t) = \sum_{l=0}^{T-t} (\lambda \gamma)^l \delta_{t+l}, \quad (22)$$

where  $\delta_t = A_t^{\theta'}(\mathbf{s}_t, \mathbf{a}_t)$ .  $\lambda \in (0, 1]$  is a discount factor. Note that (22) aims to balance the variance and bias of the advantage estimates by leveraging information from multiple future steps while discounting their influence.

If there are no constraints on the policies  $\pi_{\theta}$  and  $\pi_{\theta'}$ , significant fluctuations may occur during policy updates. This



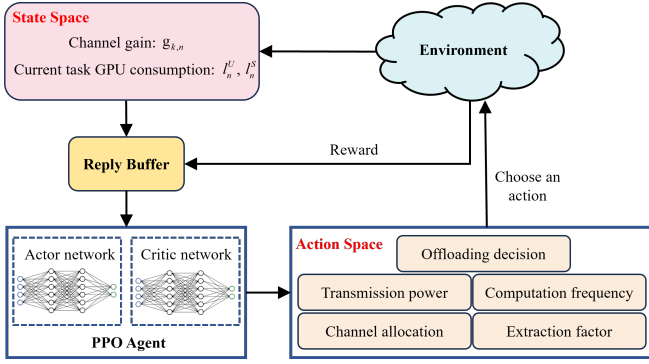


Fig. 4. The framework of the MAPPO algorithm.

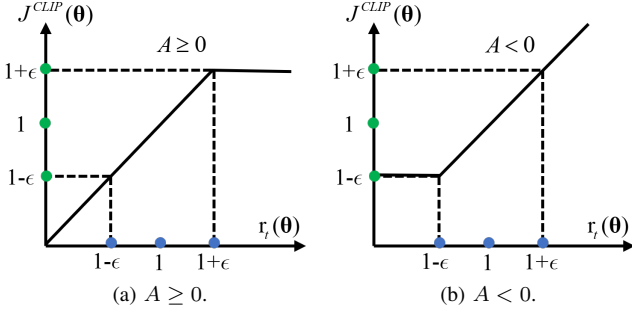


Fig. 5. The impact of  $A$  on  $J^{CLIP}$ .

is due to the limited sampling, which fails to accurately represent the probability distributions described in *Lemma 1*. To constrain the divergence between policies  $\pi_\theta$  and  $\pi_{\theta'}$ ,  $J^{CLIP}(\theta)$  is employed. It is defined as

$$J^{CLIP}(\theta) = L_t^{CLIP} = \mathbb{E}_t \left[ \min \left( r_t(\theta) A_t^{\theta'}(s_t, a_t), g(\epsilon, A_t^{\theta'}(s_t, a_t)) \right) \right], \quad (23)$$

where  $r_t(\theta) = \frac{p_\theta(a_t|s_t)}{p_{\theta'}(a_t|s_t)}$  and  $g$  is the clip function which can be defined as

$$g(\epsilon, A_t^{\theta'}(s_t, a_t)) = \begin{cases} (1 + \epsilon) A_t^{\theta'}(s_t, a_t), & \text{if } A_t^{\theta'}(s_t, a_t) \geq 0, \\ (1 - \epsilon) A_t^{\theta'}(s_t, a_t), & \text{if } A_t^{\theta'}(s_t, a_t) < 0, \end{cases} \quad (24)$$

where  $\epsilon$  is a hyperparameter, which can control the step size of the policy network updates.

Fig. 5 illustrates the impact of  $A$  on the  $J^{CLIP}$  function. Fig. 5(a) and Fig. 5(b) correspond to cases where  $A \geq 0$  and  $A < 0$ , respectively. When  $A \geq 0$ , the state-action pair is favorable, and we aim to increase its probability; that is, the larger  $p_\theta$  is, the better. However, the maximum value of  $r_t(\theta)$  cannot exceed  $1 + \epsilon$ , meaning the ratio of  $p_\theta$  to  $p_{\theta'}$  should not exceed  $1 + \epsilon$ . When  $A < 0$ , the state-action pair is unfavorable, and we aim to reduce  $p_\theta$ , but the ratio of  $p_\theta$  to  $p_{\theta'}$  should not fall below  $1 - \epsilon$ . By using the CLIP function, the difference between  $p_\theta$  and  $p_{\theta'}$  is moderate, which helps improve the model's convergence speed and performance. The loss function of the critic network aims

### Algorithm 1 MAPPO Training Algorithm

**Initialization:** Initialize the policy network with parameters  $\theta$ , the demonstration policy network with parameters  $\theta'$  and the critic network with parameters  $\phi$ . Initialize the observation space  $o_n$  and the action space  $a_n$ .

**Input:** Corresponding channel gain  $g_{k,n}$  and task queue  $Q_n$ .

**Output:** Trained neural network.

```

1: for episodes do
2:    $\pi_{\theta'} \leftarrow \pi_\theta$ ;
3:   Run policy  $\pi_{\theta'}$  for  $T$  steps and save the trajectory  $\tau$  to the replay buffer;
4:   Calculate  $T$  step GAE  $A_1^{GAE}, \dots, A_T^{GAE}$  using  $\pi_{\theta'}$  and  $\phi$ ;
5:   for epoches do
6:     Update  $\theta$  using (27);
7:     Update  $\phi$  using (28);
8:   end for
9: end for
```

to minimize the discrepancy between the state-value function and the cumulative reward and is expressed as

$$L_t^{CL} = \left\| V_t^{\theta'}(s_t) - R_t(\tau) \right\|^2. \quad (25)$$

To enhance the stochasticity of the policy, the final loss function for the MAPPO algorithm is formulated as

$$L_t^{CL+CLIP+S}(\theta) = \mathbb{E}_t \left[ L_t^{CLIP} - b_1 L_t^{CL} + b_2 H(\pi_\theta(\cdot | s_t)) \right], \quad (26)$$

where  $b_1$  and  $b_2$  are weight coefficients.  $H$  is the entropy bonus to ensure sufficient exploration.

Actor-critic based PPO algorithm comprises a policy network  $\theta$  for outputting actions and a critic network  $\phi$ . The parameters  $\theta$  are updated by

$$\arg \max_{\theta} \hat{\mathbb{E}}_t \left[ L_t^{CLIP} + b_2 H(\pi_\theta(\cdot | s_t)) \right], \quad (27)$$

and parameters  $\phi$  are updated by

$$\arg \min_{\phi} \hat{\mathbb{E}}_t \left[ L_t^{CL} \right]. \quad (28)$$

The expectation  $\hat{\mathbb{E}}_t$  is estimated using data obtained from interactions between the agent and the environment. Monte Carlo sampling is utilized to approximate the expectation  $\hat{\mathbb{E}}$ .

## IV. SIMULATION RESULTS

In this section, the performance of the semantic-aware multi-task offloading model will be demonstrated. We provide specific implementation details, investigate the QoE performance of the proposed approach, and examine the impact of user preferences on the system.

### A. Implementation Details

Three tasks are considered: text classification, image classification, and VQA, corresponding to text, image, and multi-modal tasks, respectively. For text classification, we use the SST-2 dataset, for image classification, the CIFAR-10 dataset, and for VQA, the VQAv2 dataset is adopted. The text semantic extraction network utilizes an advanced BERT-based [45] text embedding model, while the image semantic extraction network is based on the Vision Transformer (ViT) [46]. For VQA, the encoder architecture employs BERT for linguistic processing and ViT for visual feature extraction, with cross-modal fusion and answer generation performed at the receiver.

TABLE II  
SIMULATION PARAMETERS

Parameter	Value
Number of UEs $N$	4
Sub-channel bandwidth $B$	10 MHz
Task queue length $Q_n$	20
Noise power $\sigma_z^2$	2 mW
Transmit power $p_n$ range	(10, 90) mW
Semantic extraction factor $\mu_n$	(0.1, 1)
The number of user CUDA cores	1280
Local GPU frequency $f_n$ range	(1.5, 1.7) GHz
The number of ES CUDA cores	65536
Remote GPU frequency $f_s$	2.2 GHz
Energy consumption coefficient of UEs $\alpha^U$	$1 \times 10^{-26}$
Energy consumption of ES $\alpha^S$	$1.2 \times 10^{-26}$
Minimum accuracy requirements $\epsilon_{\min}$	50%
Execution latency constraint $t_{\max}$	5 ms
Training episode of the MAPPO algorithm	300
Testing episode of the MAPPO algorithm	200
Batch size of training the MAPPO	2
Epoch of training the MAPPO	5
Learning rate	$1 \times 10^{-4}$
Advantage discount factor $\lambda$	0.95
Reward discount factor $\gamma$	0.99
PPO-Clip parameter $\epsilon$	0.2
Policy entropy bonus weight $b_2$	0.1

Training is conducted using the AdamW optimizer, with a learning rate of  $3 \times 10^{-5}$ , a batch size of 50, and a weight decay of  $1 \times 10^{-4}$ . All experiments were conducted on a platform equipped with an NVIDIA RTX 4090 and a CPU Intel i9-13900K @5.8 GHz. When the training of all semantic transmission models is complete, we can calculate the GPU consumption for basic semantic extraction  $l_n^{SE}$  and the GPU consumption  $l^S$  for execution at the ES.

We consider scenarios with four UEs and orthogonal sub-carriers, where each UE has a queue length of 20, containing tasks from different task types. Additional details regarding the wireless environment, GPU computational frequency, and the proposed semantic-aware MAPPO algorithm training configurations are summarized in Table II. To verify the effectiveness of the semantic-aware multi-task offloading framework, we consider the following benchmarks:

- **Semantic-unaware MAPPO:** The benchmark transmits all data without semantic extraction during offloading, i.e.  $\mu_n = 1$ . All other settings are identical to those used in semantic-aware MAPPO.
- **Semantic-aware Dueling Double DQN (D3QN):** D3QN can only handle discrete action spaces, so we discretized the action space and used the same environment as semantic-aware MAPPO.
- **Semantic-unaware D3QN:** This benchmark transmits all data without semantic extraction during offloading, i.e.  $\mu_n = 1$ . All other settings are identical to those used in semantic-aware D3QN.
- **Local:** All tasks are executed locally.

All experimental results are averaged over 200 test runs to mitigate the effects of uneven task type distribution and dynamic changes in the channel.

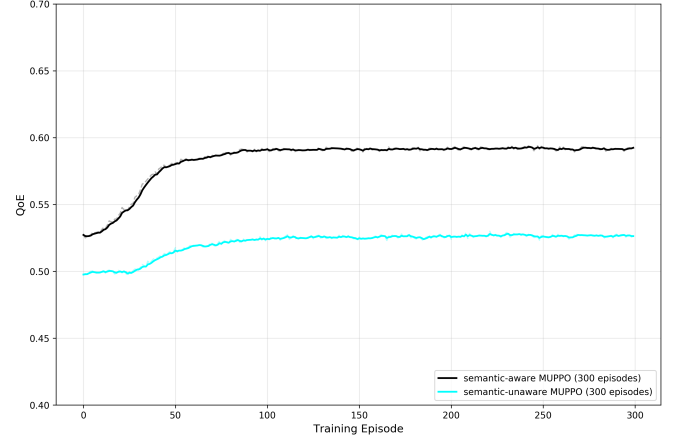


Fig. 6. Convergence of the MAPPO reward.

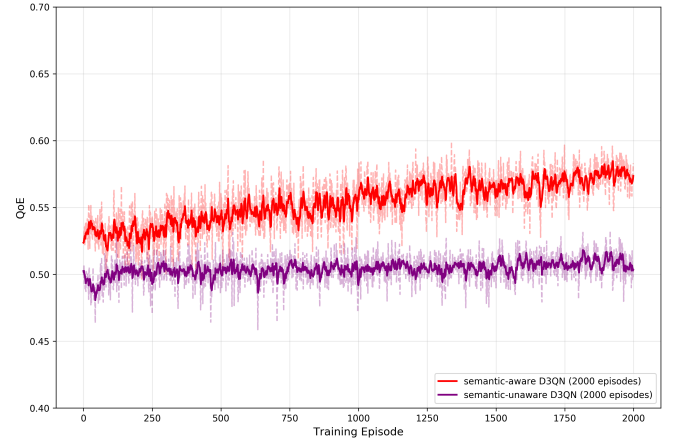


Fig. 7. Convergence of the D3QN reward.

## B. QoE Performance and Convergence

1) *Convergence Performance:* The preference parameters,  $\omega_t$ ,  $\omega_e$ , and  $\omega_a$  are all set to 1/3, indicating that the model has no specific preference among latency, energy consumption, and accuracy. Fig. 6 shows that the proposed MAPPO algorithm converges after approximately 100 episodes and maintains optimal performance. For the D3QN algorithm, the replay buffer size is set to 30000. Fig. 7 shows that the D3QN algorithm finally converges after 2000 episodes. The proposed MAPPO algorithm directly optimizes cumulative returns through policy gradient methods, while employing a trust region mechanism to constrain policy update magnitudes, thereby preventing training instability caused by abrupt policy changes. In contrast, the D3QN algorithm relies on TD learning and demonstrates lower learning efficiency in environments with sparse rewards or delayed feedback. Furthermore, to enhance the sampling efficiency of on-policy algorithms, the proposed MAPPO algorithm employs multi-threaded asynchronous sampling and completes state collection and synchronization during network updates. Consequently, the proposed MAPPO algorithm achieves faster convergence with greater stability compared to D3QN.

2) *QoE Performance:* Fig. (8) reveals the relationship



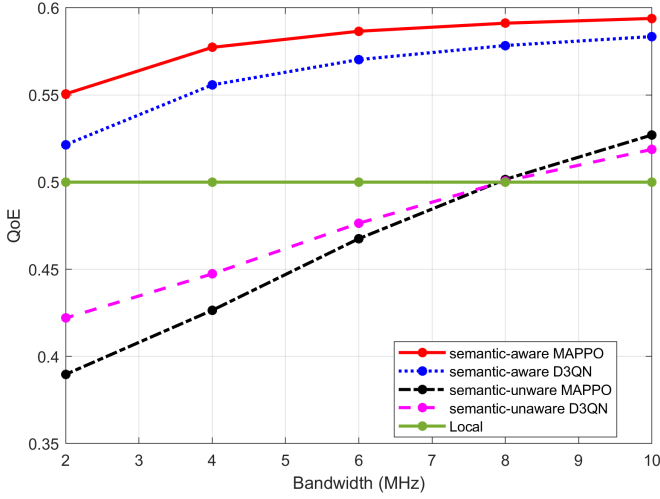


Fig. 8. QoE with different sub-carrier bandwidths.

between QoE and the sub-carrier bandwidth for UEs. All schemes are initially trained at a sub-carrier bandwidth of 10 MHz and then tested under various bandwidth conditions. It is observed that the proposed semantic-aware MAPPO algorithm achieves the best performance across all bandwidth conditions. Comparative evaluations demonstrate 12.68% QoE improvements versus semantic-unaware MAPPO and 14.48% superiority versus semantic-unaware D3QN. Semantic-unaware methods fix  $\mu_n = 1$  to transmit all data without compression, increasing transmission and execution latency, consequently degrading QoE. The D3QN algorithm requires discrete action space approximation, which may introduce quantization errors or reduce sampling efficiency. In contrast, the proposed MAPPO algorithm directly outputs continuous action probability distributions, eliminating the need for discretization and thereby avoiding the curse of dimensionality in high-dimensional action spaces. Consequently, our method achieves superior QoE. Local execution is solely related to the local computation frequency. When calculating QoE, the local computation frequency is fixed, meaning we use the local execution's latency, energy consumption, and accuracy to normalize the latency, energy, and accuracy obtained from other methods. Thus, the QoE of local execution is fixed at 0.5.

Fig. (9) describes how QoE varies with channel noise intensity. All schemes are first trained under the noise intensity of 10 mW and then tested at different noise intensities. Similarly, the proposed semantic-aware MAPPO algorithm performs better than all other benchmarks. The semantic-aware algorithm dynamically selects optimal semantic extraction factors based on real-time noise intensity and channel gain, maintaining stable QoE without significant degradation even under increasing noise levels. In contrast, semantic-unaware schemes lack adaptive semantic symbol quantity regulation, resulting in substantial performance deterioration. Fig. (10) illustrates the QoE trend versus the number of users. As the number of users increases, the server must handle more computation offloading requests, leading to elevated processing latency and energy consumption, which collectively degrade overall QoE.

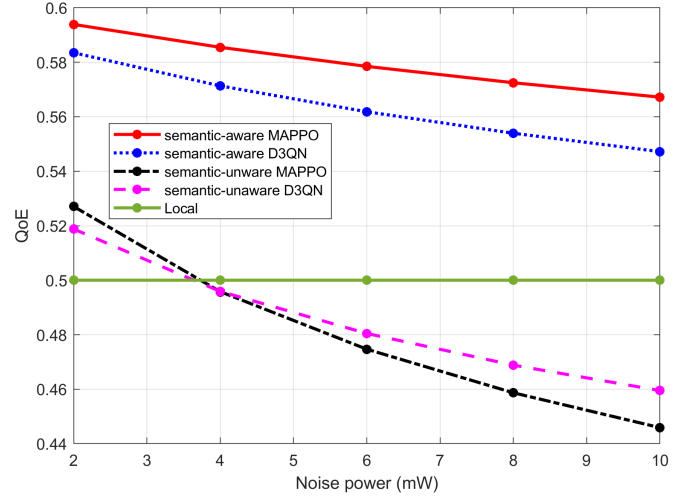


Fig. 9. QoE with different noise powers.

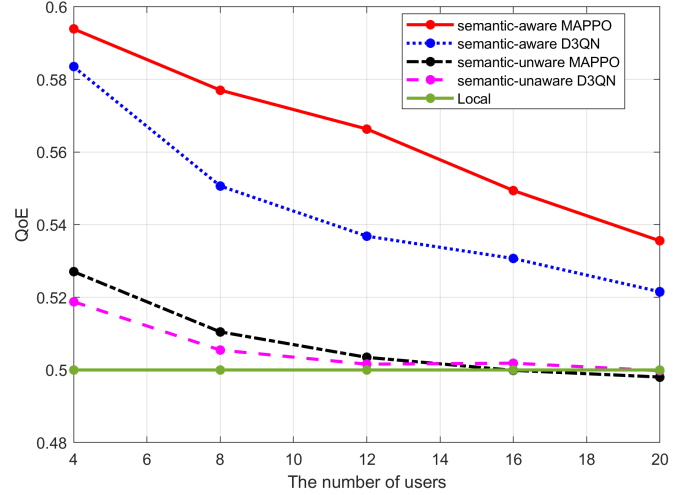


Fig. 10. QoE with different numbers of users.

Semantic-unaware approaches cannot leverage semantic extraction to reduce uplink latency during user scaling, ultimately forcing all users to execute tasks locally. Consequently, its QoE converges to the local computing baseline. Fig. (11) illustrates the QoE variation versus  $\mu_n$ . While trained at  $\mu_n = 0.1$ , the system is evaluated across varying  $\mu_n$ . Results demonstrate that when users have fewer selectable semantic extraction factors, the inability to utilize smaller compression factors for data size reduction significantly impairs channel adaptation under poor conditions, ultimately degrading QoE.

To further investigate the contributions of latency, energy consumption, and task performance to QoE, Fig. (12) illustrates the execution latency, energy consumption, and task accuracy. All metrics are measured under the following conditions: 10 MHz bandwidth, 2 mW noise power, and 4 users. Local task execution demonstrates longer latency and higher energy consumption, yet achieves optimal task performance. This occurs because local processing avoids performance degradation induced by semantic compression. However, the prolonged execution time incurs significant energy overhead.

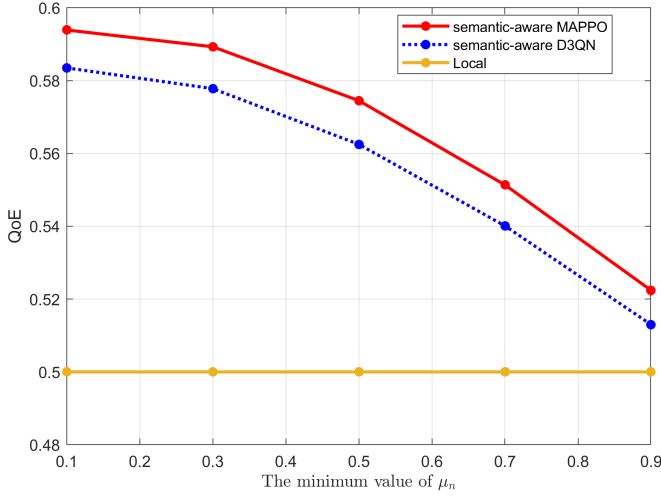


Fig. 11. QoE with different semantic extraction factor  $\mu_n$ .

TABLE III  
PERFORMANCE UNDER DIFFERENT PREFERENCES

	Delay (ms)	Energy Consumption (J)	Accuracy (%)
No Preference	0.523	0.0186	51.37
Delay Preference	<b>0.369</b>	0.0192	43.08
Energy Preference	3.50	<b>0.0163</b>	56.85
Accuracy Preference	1.67	0.0682	<b>71.99</b>

Semantic-unaware approaches exhibit inferior latency performance because of the transmission of raw task data without semantic extraction, resulting in extended transmission delays. However, server-side processing of offloaded tasks requires minimal time, yielding lower energy consumption compared to local execution. Owing to wireless channel effects during task offloading, semantic-unaware methods show slightly reduced task accuracy relative to local processing. The semantic-aware approach dynamically selects optimal semantic extraction factors based on real-time channel conditions, computational load, and transmission requirements, achieving the best trade-off among latency, energy efficiency, and task accuracy. Consequently, it delivers the highest QoE.

Fig. (13) presents the latency, energy consumption, and task performance across different task queue configurations. The system was initially trained on hybrid task scenarios and subsequently evaluated under four distinct test conditions: hybrid tasks, text classification, image classification, and VQA. The results demonstrate our algorithm's strong adaptability to diverse task types. Specifically, text classification tasks exhibit the lowest latency and energy consumption while maintaining high accuracy, attributable to their smaller data volume and computational complexity. In contrast, image classification and VQA tasks require substantially more resources, resulting in higher energy expenditure and longer processing times. The hybrid task shows performance metrics that approximately equal the arithmetic mean of individual task types, confirming the algorithm's robustness. The significant performance variations observed across task categories underscore the necessity of employing locally normalized QoE metrics for fair evaluation.



Fig. 12. Performance of different metrics.

tion.

### C. QoE Preference

We can adjust the model to achieve desired results by modifying QoE preferences for different metrics. Table III shows the performance in execution latency, energy consumption, and task accuracy under varying preference settings. Specifically, we adjust the relative magnitude of  $\omega_t$ ,  $\omega_e$ , and  $\omega_a$  to set preferences for different metrics and retrain to obtain the corresponding model for each. 1) For the delay-preference model, we set  $\omega_t = 1$ ,  $\omega_e = 0$ , and  $\omega_a = 0$ . The delay-preference model tends to choose a smaller  $\mu_n$  to reduce the amount of data transmitted. This results in a partial loss of semantic information, causing a decline in task accuracy. 2) For the energy-preference model, we set  $\omega_t = 0$ ,  $\omega_e = 1$  and  $\omega_a = 0$ . The energy-preference model prioritizes reduction of local processing energy by favoring larger semantic extraction factors, achieving significant energy savings at the cost of substantially increased transmission latency. 3) For the accuracy-preference model, we set  $\omega_t = 0$ ,  $\omega_e = 0$ , and  $\omega_a = 1$ . The accuracy-preference model aims to maximize the accuracy of all tasks, prompting it to execute locally. Nevertheless, Local task execution exhibits significantly higher latency and energy consumption.

Fig. 14 shows the performance of latency and task accuracy under different weights by adjusting the weights assigned to latency and accuracy. As the weight for latency increases, tasks are offloaded to the ES with more powerful processing capabilities, and there tends to be a preference for a smaller semantic extraction factor,  $\mu_n$ , to maximize the compression rate. This

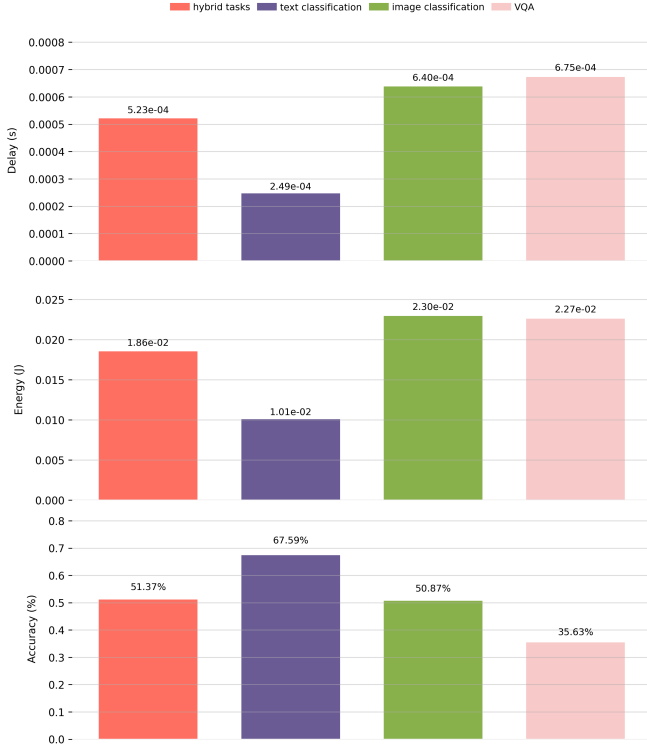


Fig. 13. Performance with different task types.

results in a decrease in the accuracy of tasks executed by the ES. Fig. 15 presents the performance of energy consumption and task accuracy under different weights. A significant jump occurs at (0.8, 0.2) when the weight for accuracy increases, as tasks are executed locally, causing a substantial increase in energy consumption and a corresponding rise in accuracy. Fig. 16 describes the performance of energy consumption and latency under varying weights. When the weight for latency increases beyond (0.3, 0.7), latency begins to decrease, and energy consumption increases. This is due to an increase in the number of tasks offloaded to the ES, and users tend to choose a smaller semantic extraction factor,  $\mu_n$ , to reduce data transmission volume. However, a smaller  $\mu_n$  means that users need more computational resources to extract more compact semantic information.

## V. CONCLUSION

In this paper, we proposed a new multi-task offloading system and designed a unified quality of experience (QoE) metric to measure overall task offloading performance. Text classification, image classification, and visual question answering (VQA) tasks can be executed locally or offloaded to the edge server after semantic extraction. A semantic-aware multi-agent PPO reinforcement learning algorithm is used to solve the problem of maximizing overall user QoE through the joint optimization of the semantic extraction factor, computing resources, and communication resources. Experimental results show that the proposed method outperforms other benchmarks in overall user QoE. Specifically, the proposed algorithm demonstrates a 12.68% improvement in QoE compared to

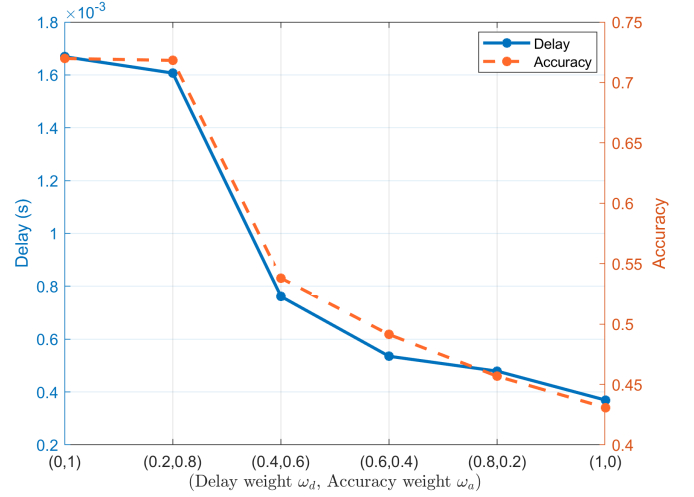


Fig. 14. Delay and accuracy performance with different weights.

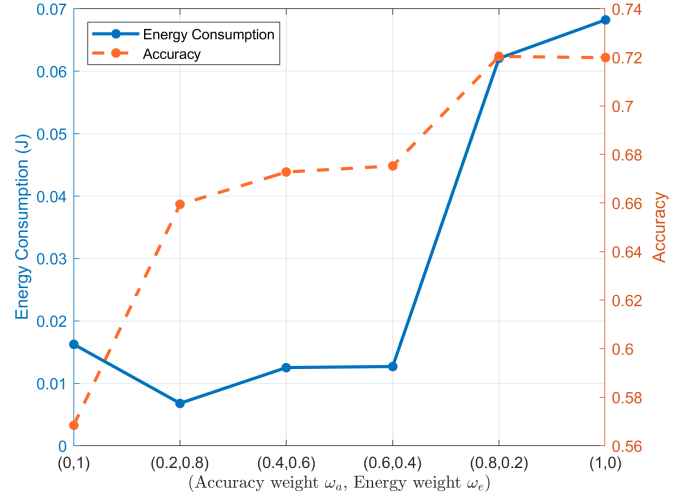


Fig. 15. Energy consumption and accuracy performance with different weights.

the semantic-unaware approach. Additionally, the proposed approach can be flexibly adapted to user preferences, fully satisfying latency, energy, and task performance preference requirements.

## REFERENCES

- [1] I. A. Elgendy, W.-Z. Zhang, C.-Y. Liu, and C.-H. Hsu, "An Efficient and Secured Framework for Mobile Cloud Computing," *IEEE Transactions on Cloud Computing*, vol. 9, no. 1, pp. 79–87, 2021.
- [2] S. Zhu, C. Liu, and Z. Xu, "High-Definition Video Compression System Based on Perception Guidance of Salient Information of a Convolutional Neural Network and HEVC Compression Domain," *IEEE Transactions on Circuits and Systems for Video Technology*, vol. 30, no. 7, pp. 1946–1959, 2020.
- [3] L. Xia, Y. Sun, C. Liang, D. Feng, R. Cheng, Y. Yang, and M. A. Imran, "WiserVR: Semantic Communication Enabled Wireless Virtual Reality Delivery," *IEEE Wireless Communications*, vol. 30, no. 2, pp. 32–39, 2023.
- [4] M. M. Rathore, A. Paul, W.-H. Hong, H. Seo, I. Awan, and S. Saeed, "Exploiting IoT and Big Data Analytics: Defining Smart Digital City Using Real-Time Urban Data," *Sustainable Cities and Society*, vol. 40, pp. 600–610, 2018.

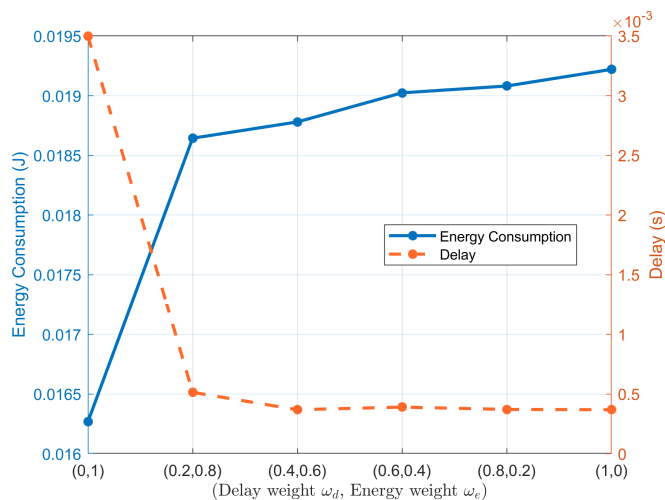


Fig. 16. Energy consumption and delay performance with different weights.

- [5] W. Weaver, "Recent Contributions to The Mathematical Theory of Communication," *ETC: A Review of General Semantics*, vol. 10, no. 4, pp. 261–281, 1953.
- [6] H. Xie and Z. Qin, "A Lite Distributed Semantic Communication System for Internet of Things," *IEEE Journal on Selected Areas in Communications*, vol. 39, no. 1, pp. 142–153, 2021.
- [7] H. Q. Xie, Z. J. Qin, G. Y. Li, and B. H. Juang, "Deep Learning Enabled Semantic Communication Systems," *IEEE Transactions on Signal Processing*, vol. 69, pp. 2663–2675, 2021.
- [8] Y. N. Wang, M. Z. Chen, T. Luo, W. Saad, D. Niyato, H. V. Poor, and S. G. Cui, "Performance Optimization for Semantic Communications: An Attention-Based Reinforcement Learning Approach," *IEEE Journal on Selected Areas in Communications*, vol. 40, no. 9, pp. 2598–2613, 2022.
- [9] E. Boursoulatz, D. B. Kurka, and D. Gündüz, "Deep Joint Source-Channel Coding for Wireless Image Transmission," *IEEE Transactions on Cognitive Communications and Networking*, vol. 5, no. 3, pp. 567–579, 2019.
- [10] D. Huang, F. Gao, X. Tao, Q. Du, and J. Lu, "Toward Semantic Communications: Deep Learning-Based Image Semantic Coding," *IEEE Journal on Selected Areas in Communications*, vol. 41, no. 1, pp. 55–71, 2023.
- [11] H. Zhang, H. Wang, Y. Li, K. Long, and A. Nallanathan, "DRL-Driven Dynamic Resource Allocation for Task-Oriented Semantic Communication," *IEEE Transactions on Communications*, vol. 71, no. 7, pp. 3992–4004, 2023.
- [12] L. Galteri, M. Bertini, L. Seidenari, T. Uricchio, and A. Del Bimbo, "Increasing Video Perceptual Quality with GANs and Semantic Coding," in *Proceedings of the 28th ACM International Conference on Multimedia*. Seattle, WA, USA: Association for Computing Machinery, 2020, p. 862–870.
- [13] P. Jiang, C. K. Wen, S. Jin, and G. Y. Li, "Wireless Semantic Communications for Video Conferencing," *IEEE Journal on Selected Areas in Communications*, vol. 41, no. 1, pp. 230–244, 2023.
- [14] S. Wang, J. Dai, Z. Liang, K. Niu, Z. Si, C. Dong, X. Qin, and P. Zhang, "Wireless Deep Video Semantic Transmission," *IEEE Journal on Selected Areas in Communications*, vol. 41, no. 1, pp. 214–229, 2023.
- [15] Y. Lin, H. Du, D. Niyato, J. Nie, J. Zhang, Y. Cheng, and Z. Yang, "Blockchain-Aided Secure Semantic Communication for AI-Generated Content in Metaverse," *IEEE Open Journal of the Computer Society*, vol. 4, pp. 72–83, 2023.
- [16] L. Xia, Y. Sun, C. Liang, D. Feng, R. Cheng, Y. Yang, and M. A. Imran, "WiserVR: Semantic Communication Enabled Wireless Virtual Reality Delivery," *IEEE Wireless Communications*, vol. 30, no. 2, pp. 32–39, 2023.
- [17] H. Du, J. Wang, D. Niyato, J. Kang, Z. Xiong, and D. I. Kim, "AI-Generated Incentive Mechanism and Full-Duplex Semantic Communications for Information Sharing," *IEEE Journal on Selected Areas in Communications*, vol. 41, no. 9, pp. 2981–2997, 2023.
- [18] Z. Tian, H. Vo, C. Zhang, G. Min, and S. Yu, "An Asynchronous Multi-Task Semantic Communication Method," *IEEE Network*, vol. 38, no. 4, pp. 275–283, 2024.
- [19] G. Zhang, Q. Hu, Z. Qin, Y. Cai, G. Yu, and X. Tao, "A Unified Multi-Task Semantic Communication System for Multimodal Data," *IEEE Transactions on Communications*, vol. 72, no. 7, pp. 4101–4116, 2024.
- [20] H. Xie, Z. Qin, X. Tao, and K. B. Letaief, "Task-Oriented Multi-User Semantic Communications," *IEEE Journal on Selected Areas in Communications*, vol. 40, no. 9, pp. 2584–2597, 2022.
- [21] A. C. Baktir, A. Ozgovde, and C. Ersoy, "How Can Edge Computing Benefit From Software-Defined Networking: A Survey, Use Cases, and Future Directions," *IEEE Communications Surveys & Tutorials*, vol. 19, no. 4, pp. 2359–2391, 2017.
- [22] X. Deng, J. Li, L. Shi, Z. Wei, X. Zhou, and J. Yuan, "Wireless Powered Mobile Edge Computing: Dynamic Resource Allocation and Throughput Maximization," *IEEE Transactions on Mobile Computing*, vol. 21, no. 6, pp. 2271–2288, 2022.
- [23] Y. Mao, J. Zhang, S. H. Song, and K. B. Letaief, "Power-Delay Tradeoff in Multi-User Mobile-Edge Computing Systems," in *2016 IEEE Global Communications Conference (GLOBECOM)*, Washington DC, USA, Conference Proceedings, pp. 1–6.
- [24] C. F. Liu, M. Bennis, M. Debbah, and H. V. Poor, "Dynamic Task Offloading and Resource Allocation for Ultra-Reliable Low-Latency Edge Computing," *IEEE Transactions on Communications*, vol. 67, no. 6, pp. 4132–4150, 2019.
- [25] S. Bi, L. Huang, H. Wang, and Y. J. A. Zhang, "Lyapunov-Guided Deep Reinforcement Learning for Stable Online Computation Offloading in Mobile-Edge Computing Networks," *IEEE Transactions on Wireless Communications*, vol. 20, no. 11, pp. 7519–7537, 2021.
- [26] M. Min, L. Xiao, Y. Chen, P. Cheng, D. Wu, and W. Zhuang, "Learning-Based Computation Offloading for IoT Devices With Energy Harvesting," *IEEE Transactions on Vehicular Technology*, vol. 68, no. 2, pp. 1930–1941, 2019.
- [27] H. Zhou, K. Jiang, X. Liu, X. Li, and V. C. M. Leung, "Deep Reinforcement Learning for Energy-Efficient Computation Offloading in Mobile-Edge Computing," *IEEE Internet of Things Journal*, vol. 9, no. 2, pp. 1517–1530, 2022.
- [28] A. Clemm, M. T. Vega, H. K. Ravuri, T. Wauters, and F. D. Turck, "Toward Truly Immersive Holographic-Type Communication: Challenges and Solutions," *IEEE Communications Magazine*, vol. 58, no. 1, pp. 93–99, 2020.
- [29] Y. Zhao, Z. Yang, X. He, X. Cai, X. Miao, and Q. Ma, "Trine: Cloud-Edge-Device Cooperated Real-Time Video Analysis for Household Applications," *IEEE Transactions on Mobile Computing*, vol. 22, no. 8, pp. 4973–4985, 2023.
- [30] Z. Qin, J. Ying, D. Yang, H. Wang, and X. Tao, "Computing Networks Enabled Semantic Communications," *IEEE Network*, pp. 1–1, 2024.
- [31] L. Yan, Z. Qin, C. Li, R. Zhang, Y. Li, and X. Tao, "QoE-Based Semantic-Aware Resource Allocation for Multi-Task Networks," *IEEE Transactions on Wireless Communications*, vol. 23, no. 9, pp. 11 958–11 971, 2024.
- [32] Y. Cang, M. Chen, Z. Yang, Y. Hu, Y. Wang, C. Huang, and Z. Zhang, "Online Resource Allocation for Semantic-Aware Edge Computing Systems," *IEEE Internet of Things Journal*, vol. 11, no. 17, pp. 28 094–28 110, 2024.
- [33] Z. Ji and Z. Qin, "Computational Offloading in Semantic-Aware Cloud-Edge-End Collaborative Networks," *IEEE Journal of Selected Topics in Signal Processing*, vol. 18, no. 7, pp. 1235–1248, 2024.
- [34] Z. Ji, Z. Qin, X. Tao, and Z. Han, "Resource Optimization for Semantic-Aware Networks With Task Offloading," *IEEE Transactions on Wireless Communications*, vol. 23, no. 9, pp. 12 284–12 296, 2024.
- [35] X. Hu, K.-K. Wong, and K. Yang, "Wireless Powered Cooperation-Assisted Mobile Edge Computing," *IEEE Transactions on Wireless Communications*, vol. 17, no. 4, pp. 2375–2388, 2018.
- [36] X. Ma, A. Zhou, S. Zhang, and S. Wang, "Cooperative Service Caching and Workload Scheduling in Mobile Edge Computing," in *IEEE INFOCOM 2020 - IEEE Conference on Computer Communications*, 2020, pp. 2076–2085.
- [37] Z. Jin, C. Zhang, Y. Jin, L. Zhang, and J. Su, "A Resource Allocation Scheme for Joint Optimizing Energy Consumption and Delay in Collaborative Edge Computing-Based Industrial IoT," *IEEE Transactions on Industrial Informatics*, vol. 18, no. 9, pp. 6236–6243, 2022.
- [38] N. Cheng, F. Chen, W. Chen, Z. Cheng, Q. Yang, C. Li, and X. Shen, "6G Omni-Scenario On-Demand Services Provisioning: Vision, Technology and Prospect," *SCIENCE CHINA Information Sciences*, vol. 54, no. 5, pp. 1025–1054, 2024.

- [39] S.-W. Ko, K. Han, and K. Huang, "Wireless Networks for Mobile Edge Computing: Spatial Modeling and Latency Analysis," *IEEE Transactions on Wireless Communications*, vol. 17, no. 8, pp. 5225–5240, 2018.
- [40] P. Mach and Z. Becvar, "Mobile Edge Computing: A Survey on Architecture and Computation Offloading," *IEEE Communications Surveys & Tutorials*, vol. 19, no. 3, pp. 1628–1656, 2017.
- [41] S. Li, J. Huang, J. Hu, and B. Cheng, "QoE-DEER: A QoE-Aware Decentralized Resource Allocation Scheme for Edge Computing," *IEEE Transactions on Cognitive Communications and Networking*, vol. 8, no. 2, pp. 1059–1073, 2022.
- [42] M. Hemmati, B. McCormick, and S. Shirmohammadi, "QoE-Aware Bandwidth Allocation for Video Traffic Using Sigmoidal Programming," *IEEE MultiMedia*, vol. 24, no. 4, pp. 80–90, 2017.
- [43] L. Yan, Z. Qin, C. Li, R. Zhang, Y. Li, and X. Tao, "QoE-based Semantic-Aware Resource Allocation for Multi-Task Networks," *IEEE Transactions on Wireless Communications*, pp. 1–1, 2024.
- [44] J. Schulman, P. Moritz, S. Levine, M. Jordan, and P. Abbeel, "High-Dimensional Continuous Control Using Generalized Advantage Estimation," *arXiv preprint arXiv:1506.02438*, 2015.
- [45] J. Devlin, M.-W. Chang, K. Lee, and K. Toutanova, "BERT: Pre-training of Deep Bidirectional Transformers for Language Understanding," in *Proceedings of the 2019 Conference of the North American Chapter of the Association for Computational Linguistics: Human Language Technologies, Volume 1 (Long and Short Papers)*. Minneapolis, Minnesota: Association for Computational Linguistics, pp. 4171–4186.
- [46] A. Dosovitskiy, L. Beyer, A. Kolesnikov, D. Weissenborn, X. Zhai, T. Unterthiner, M. Dehghani, M. Minderer, G. Heigold, S. Gelly, J. Uszkoreit, and N. Houlsby, "An Image is Worth 16x16 Words: Transformers for Image Recognition at Scale," in *International Conference on Learning Representations*, 2021.